JACS
JOURNAL OF THE AMERICAN CHEMICAL SOCIETY
Communication
pubs.acs.org/JACS

Argon Plasma Induced Phase Transition in Monolayer MoS_2

Jianqi Zhu,[†,‡] Zhichang Wang,[§] Hua Yu,[†,‡] Na Li,[†,‡] Jing Zhang,[#] JianLing Meng,[▽] Mengzhou Liao,[†,‡] Jing Zhao,[⊗] Xiaobo Lu,[†,‡] Luojun Du,[†] Rong Yang,[†,‡] Dongxia Shi,[†,‡] Ying Jiang,*[,§,∥] and Guangyu Zhang*[,†,‡,∥,⊥]

[†]Institute of Physics, Chinese Academy of Sciences, Beijing 100190, China

[‡]School of Physical Sciences, University of Chinese Academy of Sciences, Beijing 100190, China

[§]International Center for Quantum Materials, School of Physics, Peking University, Beijing 100871, China

[∥]Collaborative Innovation Center of Quantum Matter, Beijing 100190, China

[⊥]Beijing Key Laboratory for Nanomaterials and Nanodevices, Beijing 100190, China

[#]Division of Physics and Applied Physics, School of Physical and Mathematical Sciences, Nanyang Technological University, Singapore 637371

[▽]Department of Physics, Shaanxi University of Science and Technology, Xi'an 710021, China

[⊗]Beijing Institute of Nanoenery and Nanosystems, Chinese Academy of Sciences, National Center for Nanoscience and Technology (NCNST) Beijing 100083, China

Supporting Information

ABSTRACT: In this work, we report a facile, clean, controllable and scalable phase engineering technique for monolayer MoS_2. We found that weak Ar-plasma bombardment can locally induce 2H→1T phase transition in monolayer MoS_2 to form mosaic structures. These 2H→1T phase transitions are stabilized by point defects (single S-vacancies) and the sizes of induced 1T domains are typically a few nanometers, as revealed by scanning tunneling microscopy measurements. On the basis of a selected-area phase patterning process, we fabricated MoS_2 FETs inducing 1T phase transition within the metal contact areas, which exhibit substantially improved device performances. Our results open up a new route for phase engineering in monolayer MoS_2 and other transition metal dichalcogenide (TMD) materials.

Monolayer molybdenum disulfide (ML-MoS_2) is an emerging two-dimensional material with great potentials for advanced electrical and optoelectrical devices.[1−4] ML-MoS_2 has two typical phases, the so-called 2H and 1T phases.[5−8] The 2H phase is semiconducting with a band gap of ∼2.2 eV,[9] whereas the 1T phase is metallic. The structural difference between 2H and 1T phases arises from the spatial arrangement of S-atoms and the two phases can be principally converted from each other by a transversal displacement of one S-plane.[8] Engineering the phase of ML-MoS_2 is both fundamentally interesting and technically important. Mixing the two phases in a monolayer MoS_2 could principally modulate its property. In this regard, many research efforts have been devoted to develop different routes for controlling phase transition, e.g., 2H to 1T or vice versa. To date, phase transition in ML-MoS_2 can be induced by alkali metal intercalation, strain, electron beam and laser beam irradiation.[10−14] However, in general, a clean and scalable phase engineering technique is still not available.

In this paper, we report a new phase engineering route in which Ar-plasma treatment is used to activate the 2H→1T phase transition. We found that bombarding 2H-phase ML-MoS_2 with Ar ions (in plasma) carrying certain kinetic energies could effectively trigger the lateral sliding of top S-layer to form 1T-phase nanostructures. Mosaic structures consisting of both 2H and 1T phases (hereafter called 1T@2H-MoS_2) could be reliably achieved with 1T:2H ratio up to ∼40%. The atomic and electronic structure of the induced 1T phase was systematically investigated by Raman, photoluminescence (PL), X-ray photoelectron spectroscopy (XPS) and scanning tunneling microscopy (STM). This simple Ar-plasma treatment process is clean, controllable and scalable. We demonstrate the selected-area phase transition in ML-MoS_2 by taking the advantage of lithography techniques. Moreover, by inducing 1T phase transition within the metal contact areas, 2H ML-MoS_2 field effect transistor (FET) devices exhibit lower contact resistances compared to those with 2H ML-MoS_2 contacts, indicating that this technique is useful especially in large scale devices.

Figure 1a shows the schematic of the phase patterning process. Starting from 2H phase ML-MoS_2, Ar-plasma treatment on the exposed areas will induce the transition from trigonal prismatic 2H phase to the octahedral 1T phase. Note that, in this study, Ar-plasma was generated by an inductively coupled RF-plasma source and this plasma treatment is capable of 4″wafer processing (Figure S1 in Supporting Information). Very weak Ar-plasma treatments were employed with the kinetic energy of Ar ions tuned well below the level that etching effect could occur but being sufficient to wrench the S−Mo bond to induce the lateral sliding of top S-layer, in other words, the 2H→1T phase transition. Besides the plasma intensity, mainly associated with

Received: June 4, 2017
Published: July 21, 2017

DOI: 10.1021/jacs.7b05765
J. Am. Chem. Soc. 2017, 139, 10216−10219

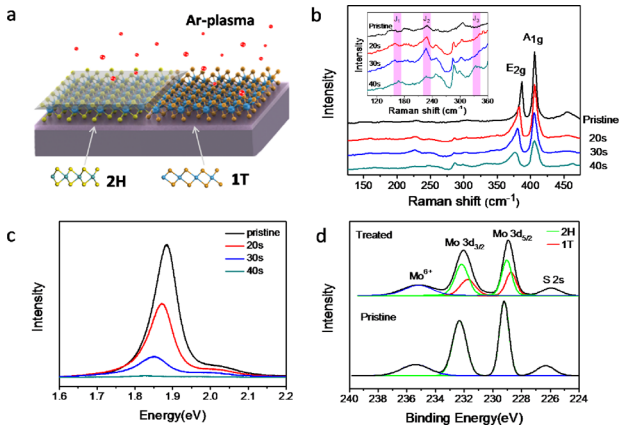

Figure 1. Formation of 1T Phase MoS_2 via plasma treatment. (a) Schematic representation of the plasma-treated process. (b) Raman spectra of ML-MoS_2 and plasma-treated MoS_2 as a function of treatment duration. New peaks can be observed in the plasma-treated monolayer MoS_2 confirming a mixture of 1T and 2H phase MoS_2. Note that different Raman intensities were observed under the same characterization conditions with 532 nm laser excitation. The inset shows enlarged spectra of new characteristic Raman peaks for the 1T phase MoS_2. (c) Time-dependent PL spectra of plasma-treated monolayer MoS_2. The PL is gradually quenched with the formation of 1T phase. (d) XPS spectra showing Mo 3d and S 2s core level peak regions for the pristine and plasma-treated MoS_2. The fitting green and red curves represent the contributions of 2H and 1T phases to the Mo 3d peaks. The lower curve is 100% 2H phase, whereas the top curve can be fitted with both 1T and 2H phase components.

the RF power and the gas pressure, the plasma treatment duration also plays a key role and will be discussed in detail.

Figure 1b,c shows optical spectroscopy characterizations of one typical ML-MoS_2 sample treated by Ar-plasma with increasing treatment duration. The pristine 2H ML-MoS_2 were grown via a chemical vapor deposition (CVD) process we developed previously.[25] Such CVD ML-MoS_2 films are polycrystalline and fully cover the SiO_2/Si substrates. Optical microscopy images of typical samples can be found in Figure S1. For the pristine as-grown ML-MoS_2, Raman spectra (Figure 1b) show characteristic peaks at 386, 406 and 454 cm^{-1}, which can be assigned to the E^1_{2g}, A_{1g} and longitudinal acoustic phonon modes, respectively.[15,16] In contrast, three weak but distinct new peaks J_1 (167 cm^{-1}), J_2 (227 cm^{-1}) and J_3 (334 cm^{-1}) appear after inducing phase transitions, in good agreement with the signature of the 1T ML-MoS_2 (inset of Figure 1b).[17−19] The continuous broadening and intensity attenuation of $E1_{2g}$ and A_{1g} bands, as a result of increasing treatment duration, suggest the growing loss of MoS_2 crystal symmetry and gradual increase of 1T-phase percentage.[20] Figure 1c shows the photoluminescence (PL) spectra of the phase-changed ML-MoS_2 under different plasma treatment duration. The pristine 2H-MoS_2 (black line) shows an optical gap of ∼1.88 eV. We can clearly see the gradual PL quenching with time evolution and the complete quenching occurs after treatment for ∼40 s. This gradual PL quenching also suggests increase of the metallic 1T-phase component.[21] Figure 1d shows the corresponding X-ray photoelectron spectroscopy (XPS) spectra. All spectra were calibrated by the C 1s peak at 284.5 eV. Peaks around 229.2 and 232.3 eV, corresponding to the Mo^{4+} $3d_{5/2}$ and Mo^{4+} $3d_{3/2}$ components in 2H-MoS_2, are shifted to lower energies after 40s Ar-plasma treatment, which is also an important evidence of the presence of the 1T phase.[22]

Atomic force microscopy (AFM) measurements on the sample surface after phase transition reveal no noticeable damages or etching effects (Figure S2 in Supporting Information). High-resolution transmission electron microscopy further confirm that the 1T and 2H phases can coexist in the same monolayer MoS_2 film (Figure S3). Within the 2H domains, both S and Mo atoms are visible; whereas within the 1T domains, only Mo atoms are visible.

To directly probe the atomic structures of the induced 1T phase, we thus carried out scanning tunnelling microscopy (STM) measurements. ML-MoS_2 samples used in STM studies were grown on highly oriented pyrolytic graphite (HOPG) substrates by CVD (Figure S4). Figure 2a shows a typical STM

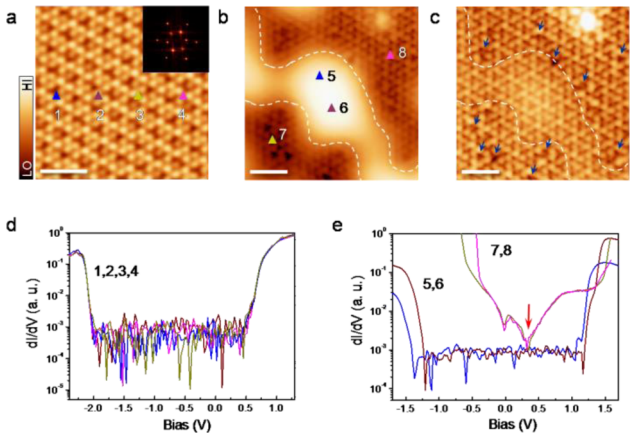

Figure 2. Atomic and electronic structure of local phase transition in monolayer MoS_2. (a−c) High-resolution STM images of monolayer MoS_2 on graphite before (a) and after (b,c) 40 s phase-transition treatment. The fast Fourier transform (FFT) of panel a is shown in the inset, where two sets of hexagonal patterns can be seen: the larger one corresponds to the top S-lattice of MoS_2, whereas the smaller one arises from the Moiré pattern. The perimeter of one bright domain is depicted by white dashed lines in panels b and c. The S-vacancies are highlighted by blue arrows in panel c. Set points of the STM images: 0.7 V, 500 pA (a); 1.5 V, 50 pA (b); 1.2 V, 5 pA (c). Scale bars in panels a−c are 1.5 nm. (d,e) dI/dV spectra in logarithmic scale recorded at different locations in panels a (triangles marked as 1,2,3,4) and b (triangles marked as 5,6,7,8), respectively. The V-shape feature is denoted by a red arrow. Set point: 1 V, 50 pA (d); 1.5 V, 50 pA (e).

image of as-grown ML-MoS_2 at a sample bias voltage of 0.6 V with the associated fast Fourier transform (FFT) in the inset. The observed hexagonal lattice corresponds to the top S-layer of the 2H-phase MoS_2. A 3.3 Å lattice constant can be revealed for MoS_2 from the line profile in Figure S4. In Figure 2a, we can also see a distinct Moiré superstructure arising from the lattice mismatch between MoS_2 and HOPG (inset of Figure 2a).[23] Figure 2b shows the STM image taken from a ML-MoS_2 sample with 40 s phase-transition treatment, where bright domains with size of a few nanometers appeared. From the atomically resolved image (Figure 2c), we can clearly see that the atomic rows are transversally displaced at the perimeter of bright domains, indicating that the bright and dark regions should correspond to different phases of ML-MoS_2. In addition, a few S-vacancies can be observed in the dark regions (see the blue arrows in Figure 2c), suggesting that the S-vacancies initiate the phase transition and stabilize the 1T phase.[14] Besides, samples after phase transition are also stable even after exposing them in ambient conditions for a week (Figure S5).

DOI: 10.1021/jacs.7b05765
J. Am. Chem. Soc. 2017, 139, 10216−10219

To clarify the electronic structure of the phase-changed ML-MoS_2, we further carried out scanning tunneling spectroscopy (STS) analysis. Figure 2d,e shows dI/dV spectra taken on the pristine and phase-changed samples as shown in Figure 2a,b, respectively. The measured electronic bandgap of pristine 2H-MoS_2 is ~2.4 eV (Figure 2d). In contrast, phase-changed samples show inhomogeneous electronic structure. The bright domains have the similar bandgap as the 2H-MoS_2, whereas the dark regions exhibit distinct metallic behavior. Therefore, 2H-domains (bright regions) and 1T-domains (dark regions) coexist at the nanometer scale. Although a substantially amount of 2H domains still exist in the phase-changed ML-MoS_2, significant charge transfer between the 2H and 1T domains could occur upon the formation of the excitons, which is responsible for the PL quenching behavior observed above. Besides, the V-shaped dI/dV spectra (see the red arrow in Figure 2e) suggest the existence of Dirac-Fermion like carries in 1T-MoS_2. Those results confirm the local 2H→1T phase transition of ML-MoS_2 via Ar-plasma treatment, which is consistent with the optical characterizations above. Furthermore, the fraction of metallic 1T phase can be up to 40% after 40 s treatment, whereas further increasing the treatment duration leads to the formation of high-concentration S-defects, which eliminates the metallic 1T phases (Figure S6 in Supporting Information).

From the mentioned discussions, we can see that this phase transition process is efficient, clean and scalable. Considering that the Ar-plasma treatment process is compatible with standard lithography techniques, we thus demonstrate the selective-area phase transition in 2H ML-MoS_2. This approach includes two steps. Patterned poly methyl methacrylate (PMMA) mask on MoS_2 was first fabricated by electron beam lithography; and Ar-plasma treatment was then performed on MoS_2 with prepatterned mask (Figure 3a). As a result, phase transition was induced on the exposed area of ML-MoS_2; whereas 2H-phase ML-MoS_2 was preserved under the PMMA covering (Figure 3b–d). The green filled squares shown in Figure 3a represent the areas covered by PMMA. After the selective-area phase transition and removal of the PMMA mask, no morphology changes can be visualized from AFM imaging (Figure 3b). Figure 3c,d is the Raman/PL mapping obtained at 332 cm^{-1} and 1.83 eV, respectively, clearly showing 1T and 2H components.

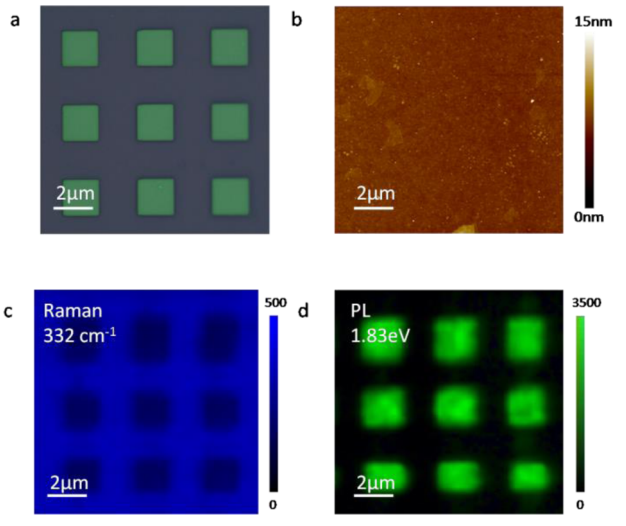

Figure 3. Characterization of a phase patterned monolayer MoS_2. (a) Optical microscopy image of the monolayer MoS_2 covered by PMMA pattern. (b) AFM image of the same MoS_2 film in panel a after phase-patterning and resist removing. (c) Raman intensity mapping near 332 cm^{-1} (1T) in panel b with a spectral width of 20 cm^{-1}. (d) PL intensity mapping near 1.83 eV of the same area as panel c, indicating the plasma-treated region.

It has been shown that inducing metallic 1T phase transition on the electrode contact areas could substantially decrease the contact resistance and improve devices' electrical performances.[24] Although our Ar-plasma treatment only locally induces 2H→1T phase transition, effective decrease of the contact resistance can still be achieved due to the percolation of the 1T domains (see Figure 2b). We thus fabricated three types of devices based on CVD ML-MoS_2 by standard lithographic, oxygen-plasma etching, metal (Au/Ti) deposition and phase-transition techniques (Figure S7).[25] Type-I devices are normal devices with 2H-channels and 2H-contacts; type-II devices have 2H-channels and 1T@2H-contacts; and type-III devices have 1T@2H-channels and1T@2H-contacts, as shown in Figure 4a.

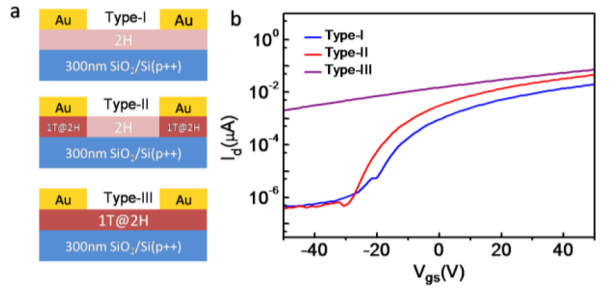

Figure 4. Performance of the device with a heterophase structure in MoS_2. (a) Schematic depiction of three types of devices. Type-I devices have 2H-channels and 2H-contacts. Type-II devices have 2H-channels and 1T@2H-contacts. Type-III devices have 1T@2H channel. (b) Transfer characteristics of back-gate monolayer MoS_2 FET measured at V_{ds} = 100 mV are shown, respectively. The type-III device with 1T@2H channel, showing an absence of gate modulation owing to the metallic character of the 1T phase.

Figure 4b shows the typical transfer characteristics of the three types devices. Large gate modulation of the 2H-channel can be seen with an On/Off ratio ~ 10^5, whereas the 1T@2H channel has much weaker gate dependence (see the purple curve in Figure 4b), which is expectable since the pure 1T-phase is metallic. We also examined many these type-III devices in different areas (Figure S8) and confirm our phase transition process is uniform. As one can see, the normalized currents with 1T@2H-phase electrodes are approximately two times higher than in devices with 2H-phase electrodes, which translates into slightly higher on/off ratios. The I_{ds}–V_{ds} curves for normal 2H-MoS_2/metal contacted (blue line) and 1T@2H-MoS_2/metal contacted (red line) devices with channel length L = 100 μm and channel width W = 10 μm shown in Figure S9. For the 1T@2H-phase contacted device, a nearly linear ohmic behavior and an obvious enhancement of the ON current can be observed.

In summary, we have developed a clean and efficient method for phase patterning in ML-MoS_2 by Ar-plasma treatments. The 2H→1T phase transition in our ML-MoS_2 samples were systematically investigated and confirmed by a variety of structural and electronic characterizations. This new approach could pave the way toward tailoring the phase in ML-MoS_2,

DOI: 10.1021/jacs.7b05765
J. Am. Chem. Soc. 2017, 139, 10216–10219

which has potential applications in electronics, optics, catalysis and energy harvesting devices.

■ ASSOCIATED CONTENT

Supporting Information

The Supporting Information is available free of charge on the ACS Publications website at DOI: 10.1021/jacs.7b05765.

Experimental procedures and Supporting Figures S1−S9 describing the additional data (PDF)

■ AUTHOR INFORMATION

Corresponding Authors

*gyzhang@aphy.iphy.ac.cn
*yjiang@pku.edu.cn

ORCID

Luojun Du: 0000-0002-7875-3817

Notes

The authors declare no competing financial interest.

■ ACKNOWLEDGMENTS

This work was supported by the National Key R&D program under Grant No. 2016YFA0300904 and 2016YFA0300901, the National Science Foundation of China (NSFC, Grant No. 61325021, 51572289, 91321309 and 11290162/A040106), the Key Research Program of Frontier Sciences, CAS under Grant No. QYZDB-SSW-SLH004, and the Strategic Priority Research Program (B), CAS under Grant No. XDB07010100.

■ REFERENCES

(1) Geim, A. K.; Grigorieva, I. V. *Nature* **2013**, *499*, 419.
(2) Voiry, D.; Yamaguchi, H.; Li, J.; Silva, R.; Alves, D. C. B.; Fujita, T.; Chen, M.; Asefa, T.; Shenoy, V. B.; Eda, G.; Chhowalla, M. *Nat. Mater.* **2013**, *12*, 850.
(3) Gong, Y.; Lin, J.; Wang, X.; Shi, G.; Lei, S.; Lin, Z.; Zou, X.; Ye, G.; Vajtai, R.; Yakobson, B. I.; Terrones, H.; Terrones, M.; Tay, B. K.; Lou, J.; Pantelides, S. T.; Liu, Z.; Zhou, W.; Ajayan, P. M. *Nat. Mater.* **2014**, *13*, 1135.
(4) Liu, B.; Chen, L.; Liu, G.; Abbas, A. N.; Fathi, M.; Zhou, C. *ACS Nano* **2014**, *8*, 5304.
(5) Chhowalla, M.; Shin, H. S.; Eda, G.; Li, L.-J.; Loh, K. P.; Zhang, H. *Nat. Chem.* **2013**, *5*, 263.
(6) Duerloo, K.-A. N.; Li, Y.; Reed, E. J. *Nat. Commun.* **2014**, *5*, 4214.
(7) Guo, Y.; Sun, D.; Ouyang, B.; Raja, A.; Song, J.; Heinz, T. F.; Brus, L. E. *Nano Lett.* **2015**, *15*, 5081.
(8) Eda, G.; Fujita, T.; Yamaguchi, H.; Voiry, D.; Chen, M.; Chhowalla, M. *ACS Nano* **2012**, *6*, 7311.
(9) Lin, Y.-C.; Dumcenco, D. O.; Huang, Y.-S.; Suenaga, K. *Nat. Nanotechnol.* **2014**, *9*, 391.
(10) Kappera, R.; Voiry, D.; Yalcin, S. E.; Branch, B.; Gupta, G.; Mohite, A. D.; Chhowalla, M. *Nat. Mater.* **2014**, *13*, 1128.
(11) Wang, L.; Xu, Z.; Wang, W.; Bai, X. *J. Am. Chem. Soc.* **2014**, *136*, 6693.
(12) Song, S.; Keum, D. H.; Cho, S.; Perello, D.; Kim, Y.; Lee, Y. H. *Nano Lett.* **2016**, *16*, 188.
(13) Enyashin, A. N.; Yadgarov, L.; Houben, L.; Popov, I.; Weidenbach, M.; Tenne, R.; Bar-Sadan, M.; Seifert, G. *J. Phys. Chem. C* **2011**, *115*, 24586.
(14) Cho, S.; Kim, S.; Kim, J. H.; Zhao, J.; Seok, J.; Keum, D. H.; Baik, J.; Choe, D.-H.; Chang, K.; Suenaga, K.; Kim, S. W.; Lee, Y. H.; Yang, H. *Science* **2015**, *349*, 625.
(15) Sun, Y.; Liu, K.; Hong, X.; Chen, M.; Kim, J.; Shi, S.; Wu, J.; Zettl, A.; Wang, F. *Nano Lett.* **2014**, *14* (9), 5329.
(16) Ding, Q.; Meng, F.; English, C. R.; Cabán-Acevedo, M.; Shearer, M. J.; Liang, D.; Daniel, A. S.; Hamers, R. J.; Jin, S. *J. Am. Chem. Soc.* **2014**, *136*, 8504.
(17) Nayak, A. P.; Pandey, T.; Voiry, D.; Liu, J.; Moran, S. T.; Sharma, A.; Tan, C.; Chen, C.; Li, L.-J.; Chhowalla, M. U.; Lin, J.-F.; Singh, A. K.; Akinwande, D. *Nano Lett.* **2015**, *15*, 346.
(18) Liu, Q.; Li, X.; He, Q.; Khalil, A.; Liu, D.; Xiang, T.; Wu, X.; Song, L. *Small* **2015**, *11*, 5556.
(19) Splendiani, A.; Sun, L.; Zhang, Y.; Li, T.; Kim, J.; Chim, C.-Y.; Galli, G.; Wang, F. *Nano Lett.* **2010**, *10*, 1271.
(20) Chou, S. S.; Huang, Y.-K.; Kim, J.; Kaehr, B.; Foley, B. M.; Lu, P.; Dykstra, C.; Hopkins, P. E.; Brinker, C. J.; Huang, J.; Dravid, V. P. *J. Am. Chem. Soc.* **2015**, *137*, 1742.
(21) Eda, G.; Yamaguchi, H.; Voiry, D.; Fujita, T.; Chen, M.; Chhowalla, M. *Nano Lett.* **2011**, *11*, 5111.
(22) Cai, L.; He, J.; Liu, Q.; Yao, T.; Chen, L.; Yan, W.; Hu, F.; Jiang, Y.; Zhao, Y.; Hu, T.; Sun, Z.; Wei, S. *J. Am. Chem. Soc.* **2015**, *137*, 2622.
(23) Lu, C.-I.; Butler, C. J.; Huang, J.-K.; Hsing, C.-R.; Yang, H.-H.; Chu, Y.-H.; Luo, C.-H.; Sun, Y.-C.; Hsu, S.-H.; Yang, K.-H. O.; Wei, C.-M.; Li, L.-J.; Lin, M.-T. *Appl. Phys. Lett.* **2015**, *106*, 181904.
(24) Ma, Y.; Liu, B.; Zhang, A.; Chen, L.; Fathi, M.; Shen, C.; Abbas, A. N.; Ge, M.; Mecklenburg, M.; Zhou, C. *ACS Nano* **2015**, *9*, 7383.
(25) Zhang, J.; Yu, H.; Chen, W.; Tian, X.; Liu, D.; Cheng, M.; Xie, G.; Yang, W.; Yang, R.; Bai, X.; Shi, D.; Zhang, G. *ACS Nano* **2014**, *8*, 6024.

DOI: 10.1021/jacs.7b05765
J. Am. Chem. Soc. 2017, 139, 10216−10219